

Generalized Space-Time Periodic Diffraction Gratings: Theory and Applications

Sajjad Taravati and George V. Eleftheriades

*The Edward S. Rogers Sr. Department of Electrical and Computer Engineering,
University of Toronto, Toronto,
Ontario M5S 3H7, Canada*

Email: sajjad.taravati@utoronto.ca

(Dated: today)

This paper studies the theory and applications of the diffraction of electromagnetic waves by space-time periodic (STP) diffraction gratings. We show that, in contrast with conventional spatially periodic grating, a STP diffraction grating produces spatial diffraction orders, each of which is formed by an infinite set of temporal diffraction orders. Such spatiotemporally periodic gratings are endowed with enhanced functionalities and exotic characteristics, such as asymmetric diffraction pattern, nonreciprocal diffraction, and enhanced diffraction efficiency. The theory of the wave diffraction by STP gratings is formulated through satisfying the conservation of both momentum and energy, and rigorous Floquet mode analysis. Furthermore, the theoretical analysis of the structure is supported by time and frequency domain FDTD numerical simulations for both transmissive and reflective STP diffraction gratings. Additionally, we provide the conditions for Bragg and Raman-Nath diffraction regimes for STP gratings. Finally, as a particular example of a practical application of the STP diffraction gratings to communication systems, we propose an original multiple access communication system featuring full-duplex operation. STP diffraction gratings are expected to find exotic practical applications in communication systems, especially for the realization of enhanced-efficiency or full-duplex beam coders, nonreciprocal beam splitters, nonreciprocal and enhanced-resolution holograms, and illusion cloaks.

I. INTRODUCTION

Light diffraction by spatially periodic structures is a fundamental phenomenon in optics and is of great importance in a variety of engineering applications [1–8]. Such spatially periodic diffraction gratings are formed by a slab with a periodic *spatial* variation at the *wavelength scale*. The form of the grating periodicity is usually sinusoidal [9, 10] or binary [11]. They exhibit unique spectral properties as the light impinging on the periodically modulated medium is reflected or transmitted at specific angles only, which in general is not the case for aperiodic media. Diffraction gratings play the main role in numerous electromagnetic systems [4, 12], including but not restricted to, holography [13, 14], beam shaping [15], data processing and optical logic [16, 17], medical diagnostic measurements [18, 19], microwave and optical spectrum analysis [3, 20, 21]

Over the past decade, STP media have spurred a huge scientific attention, due to their extraordinary interaction with electromagnetic waves [22–34]. Such media are not governed by the Lorentz reciprocity law, so that they may provide a nonreciprocal frequency generation and amplification. Analytical investigation of wave propagation and scattering in time periodic media [35, 36], and STP media [24, 26, 27, 33, 37, 38] represents an interesting topic due to the complexity and rich physics of the problem. Moreover, an interesting feature is the diverse and unique practical applications of STP media. As of today, STP structures have been used as parametric traveling-wave amplifiers [37–40], optical isolators and circulators [26, 41–46], nonreciprocal

metasurfaces [47–49], pure frequency mixers [50], antennas [51–55], impedance matching structures [56], and mixer-duplexer-antenna systems [57].

This paper presents the theoretical analysis of diffraction from a generalized STP diffraction grating. This includes the wave diffraction from the grating and the angle of transmission and reflection for each spatial-temporal diffraction order. The provided analysis is applicable to all types of periodicities. We show that, in contrast to conventional spatially periodic gratings, in a STP grating, each spatial diffraction order is composed of an infinite number of temporal harmonics, each one of which is diffracted at a certain angle of diffraction. It is demonstrated that such a STP grating provides more functionalities, such as nonreciprocal diffraction, an asymmetric diffraction pattern and inherent frequency generation, which may be used to realize new optical and communication systems with enhanced efficiency. The theoretical analysis of these STP gratings is supported by a wavevector diagram of the diffracted space-time orders. In addition, we provide the FDTD numerical simulation of the problem. We deeply investigate the difference between the wave diffraction in transmissive and reflective STP diffraction gratings, as well as the diffraction in Bragg (thick) and Raman-Nath (thin) regimes of STP gratings. Furthermore, it is shown that the modulation signal can be used for diffraction steering.

The paper is structured as follows. Section II presents the theoretical analysis of the wave diffraction from general STP diffraction gratings, and derives the diffraction angles for each space-time diffracted order. In Sec. III, we provide some illustrative examples with the FDTD

numerical simulation investigation in the time and frequency domains. This section also evaluates the effect of the grating thickness on the wave diffraction. Next, Sec. IV demonstrates the nonreciprocal diffraction by transmissive and reflective STP gratings. Section V discusses practical applications based on leveraging the unique and exotic properties of diffraction from STP gratings. Finally, Sec. VI concludes the paper.

II. THEORETICAL ANALYSIS

A. Space-time periodic (STP) diffraction grating

Figure 1(a) depicts the wave diffraction from conventional transmissive planar spatially periodic diffraction gratings. The conventional static grating in Fig. 1(a) possesses a relative electric permittivity in the region from $z = 0$ to $z = d$ given by $n_{\text{gr}}^2(x) = \epsilon_{\text{gr}}(x) = f_{\text{per}}(x)$, where $f_{\text{per}}(x)$ is a periodic function of x , e.g., a sinusoidal, binary (square), or sawtooth function. Electromagnetic waves always travel in straight lines, but when passing near an obstruction they tend to bend around that obstruction and spread out. The diffraction phenomenon occurs when an electromagnetic wave passes by a corner or through a slit or grating that has an optical size comparable to the wavelength. The diffraction by a grating is a specialized case of wave scattering, where an object with regularly repeating features yields an orderly diffraction of the electromagnetic wave in a pattern consisting of a set of diffraction orders m . As shown in Fig. 1(a), considering normal incidence of the input wave ($\theta_i = 0$), the diffraction produced by conventional transmissive static spatially periodic gratings is symmetric with respect to the periodicity (x) direction. The symmetry of the diffraction pattern includes the symmetry in both the angles of diffraction orders θ_m (e.g., $\theta_{+2} = \theta_{-2}$) and the intensity of the diffracted orders P_m (e.g., $P_{+2} = P_{-2}$). In addition, assuming a monochromatic input wave with temporal frequency ω_0 , no change in the temporal frequency of the incident field occurs, and hence, the diffracted orders share the same temporal frequency of ω_0 .

Now, consider the transmissive planar STP diffraction grating shown in Fig. 1(b). This figure shows a generic representation of the spatiotemporal diffraction from a STP diffraction grating, which is distinctly different from the spatial diffraction from a conventional space periodic diffraction grating in Fig. 1(a). The grating is interfaced with two semi-infinite dielectric regions, i.e., region 1 characterized with the refractive index n_1 and wavenumber k , and region 3 characterized with the refractive index n_3 and wavenumber k'' . The relative electric permittivity of this STP grating is periodic in both space and time, with temporal frequency Ω and spatial frequency K , given by

$$n_{\text{gr}}^2(x, t) = \epsilon_{\text{gr}}(x, t) = f(f_{1,\text{per}}(x), f_{2,\text{per}}(t)), \quad (1)$$

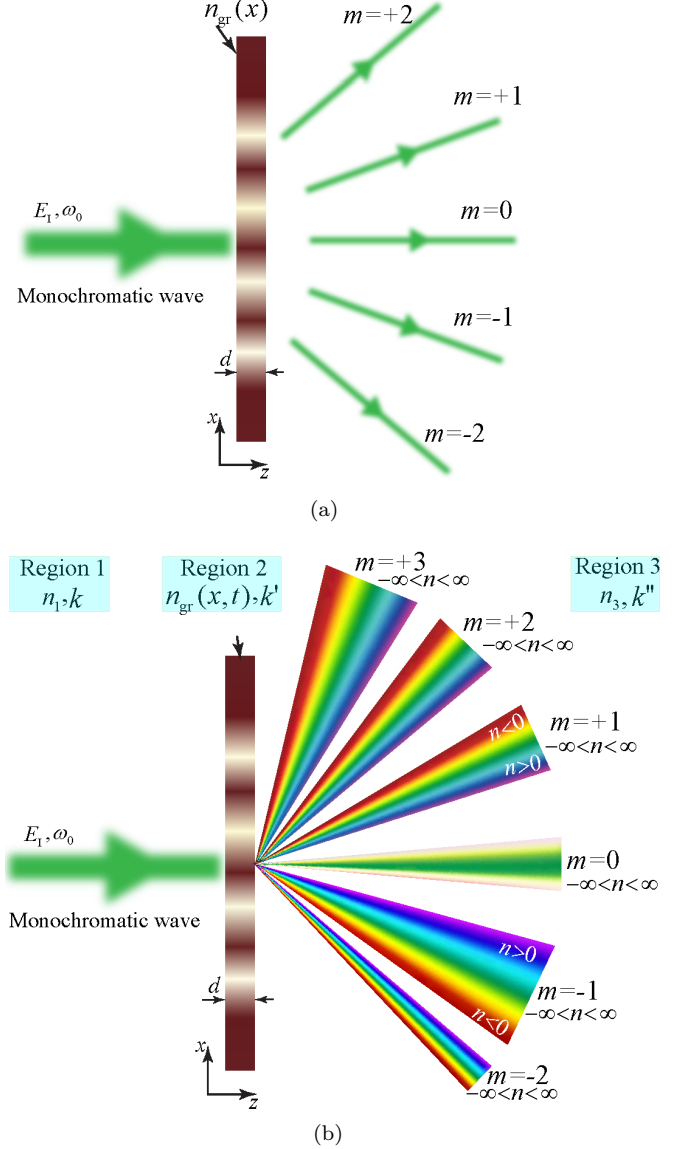


FIG. 1. Diffraction from a transmissive grating for a monochromatic incident wave. (a) Conventional spatial diffraction grating with $n_{\text{gr}}^2(x) = \epsilon_{\text{gr}}(x) = f_{\text{per}}(x)$, where spatial diffraction orders (e.g. $-2 < m < 2$) share the same temporal frequency, i.e., ω_0 , with the input wave. (b) Generalized STP diffraction grating, i.e., $n_{\text{gr}}^2(x, t) = \epsilon_{\text{gr}}(x, t) = f(f_{1,\text{per}}(x), f_{2,\text{per}}(t))$, where each m th spatial diffraction order (e.g., $-2 < m < 3$) is formed by an infinite number of temporal diffraction orders $\omega_0 + n\Omega$ with $-\infty < n < \infty$.

where $f_{1,\text{per}}(x)$ and $f_{2,\text{per}}(t)$ are periodic functions of space (in the x direction) and time, respectively. The wavenumber in region 2 (inside the STP grating) is denoted by k' .

Assuming normal (or oblique) incidence of the input wave, the transmissive dynamic spatiotemporally periodic gratings (shown in Fig. 1(b)) produces a diffraction

pattern which, in contrast to the conventional gratings, is not symmetric with respect to the periodicity (x) direction. The asymmetry of the diffraction pattern extends to both the diffraction angles of diffracted orders θ_m (e.g., $\theta_{m=+2} \neq \theta_{m=-2}$) and the intensities of the diffracted orders P_m (e.g., $P_{m=+2} \neq P_{m=-2}$). Furthermore, the time-variation of the grating (with frequency Ω) results in the generation of new frequencies. Hence, assuming a monochromatic input wave with temporal frequency ω_0 , an infinite set of temporal frequencies will be generated inside the grating and will be diffracted, so that each spatial diffracted order (m) is composed of an infinite number of temporal diffraction orders n . As a result, for such a generalized STP diffraction grating, the diffraction characteristics are defined for each spatial-temporal diffracted order (mn) so that the diffracted order (mn) is transmitted at a specified angle θ_{mn} attributed to the electric field E_{mn}^T .

To best investigate the wave diffraction by a space-time-varying grating, we first study the interaction of the electromagnetic wave with space and time interfaces, separately. Figure 2(a) sketches the Minkowski space-time diagram of a spatial interface between two media of refractive indices n_1 and n_2 , respectively, in the plane (z, ct). This figure shows scattering of forward and backward fields and conservation of energy and momentum for different scenarios. The temporal axis of the Minkowski space-time diagram is scaled with the speed of light c , and therefore is labeled by ct for changing the dimension of the addressed physical quantity from time to length, in accordance to the dimension associated to the spatial axes labeled z . This problem represents the conventional case of electromagnetic wave incidence and scattering from a spatial (static) interface, where $n(z < 0) = n_1$ and $n(z > 0) = n_2$. At this spatial boundary, the normal magnetic field \mathbf{B} , the normal electric field displacement \mathbf{D} , and the temporal frequency are preserved, but the wavenumber k changes, i.e., energy is preserved but momentum changes. As a result, the wavenumber of the forward transmitted wave in the region 2 corresponds to $k_t^+ = n_1 k_i^+ / n_2$, whereas the temporal frequency of the transmitted wave in region 2 is equal to that of the region 1, i.e., $\omega_t = \omega_i$.

Figure 2(b) shows the space-time diagram of a time interface between two media of refractive indices n_1 and n_2 , which is the dual case of the spatial slab in Fig. 2(a) [58–60]. Here, the refractive index suddenly changes from one value (n_1) to another (n_2) at a given time throughout all space, i.e., $n(t < 0) = n_1$ and $n(t > 0) = n_2$. The temporal change of the refractive index produces both reflected (backward) and transmitted (forward) waves, which is analogous to the reflected and transmitted waves produced at the spatial interface between two different media in Fig. 2(a). The total charge Q and the total flux ψ must remain constant at the moment of the jump from n_1 to n_2 , implying that both transversal and normal components of \mathbf{D} and \mathbf{B} do not change instantaneously [61, 62], which is different than the static case

(shown in Fig. 2(a)) where only normal components of the magnetic field \mathbf{B} and electric field displacement \mathbf{D} are conserved. Specifically, at a time interface, the magnetic field \mathbf{B} , the electric field displacement \mathbf{D} and the wavenumber k are preserved. This yields a change in the temporal frequency of the incident wave so that the frequency of the forward transmitted wave in the region 2 corresponds to $\omega_t^+ = n_1 \omega_i^+ / n_2$, i.e., where momentum is preserved but energy changes.

Figure 2(c) depicts the space-time diagram of a spatial-temporal interface, i.e., $n(z/c + t < 0) = n_1$ and $n(z/c + t > 0) = n_2$, as the combination of the space and time interfaces in Figs. 2(a) and 2(b), respectively. It may be seen that the spatial-temporal interface resembles the spatial interface configuration in Fig. 2(a) in the region $n = n_1$ and the temporal interface configuration in Fig. 2(b) for $n = n_2$. Here, only one of the four forward and backward waves reaches the interaction point from the past, whereas the other three waves travel from the interface in the positive time direction [25, 59, 63]. At such a spatial-temporal interface, normal component of the magnetic field \mathbf{B} and normal component of the electric field displacement \mathbf{D} are preserved [64, 65]. However, both the spatial frequency (wavenumber) k and the temporal frequency changes, i.e., both momentum and energy change. For a periodic space-time-modulated medium, as in Fig. 1(b), the same phenomenon, i.e., a change in the spatial and temporal frequencies occurs for each interface. Hence, following the Floquet theorem, a STP grating introduces an infinite number of space and time diffraction orders, as it is described in Sec. II B.

B. Diffraction angles

Figure 3 shows a generic illustration example of a wavevector isofrequency diagram for the diffraction from a STP diffraction grating. The grating is characterized with the spatial frequency K (the spatial periodicity of the STP grating reads $\Lambda = 2\pi/K$) and the temporal frequency Ω . Figure 3 sketches the phase matching of spatial-temporal harmonic components of the total field inside the grating with propagating backward diffracted orders in region 1, and forward diffracted orders in region 3. We assume the grating is interfaced with two semifinite dielectrics, i.e., $z \rightarrow -\infty < \text{region 1} < z = 0$ and $d < \text{region 3} < z \rightarrow \infty$, respectively. Region 1, region 2 (inside the STP grating) and region 3 are, respectively, characterized with the phase velocities $v_r = c/n_1$, $v_r' = c/n_{av}$ and $v_r'' = c/n_3$, and the wavevectors $\mathbf{k}_{mn} = k_{x,mn}\hat{\mathbf{x}} + k_{z,mn}\hat{\mathbf{z}}$, $\mathbf{k}'_{pmn} = k'_{x,pmn}\hat{\mathbf{x}} + k'_{z,pmn}\hat{\mathbf{z}}$, and $\mathbf{k}''_{mn} = k''_{x,mn}\hat{\mathbf{x}} + k''_{z,mn}\hat{\mathbf{z}}$. Here, c represents the velocity of the light in the vacuum, m and n denote the number of the space and time harmonics, respectively, while p represents the number of the mode in region 2, inside the grating (these modes only exist inside the grating, and Sec. II D elaborates on their properties).

The STP grating assumes oblique incidence of a y -

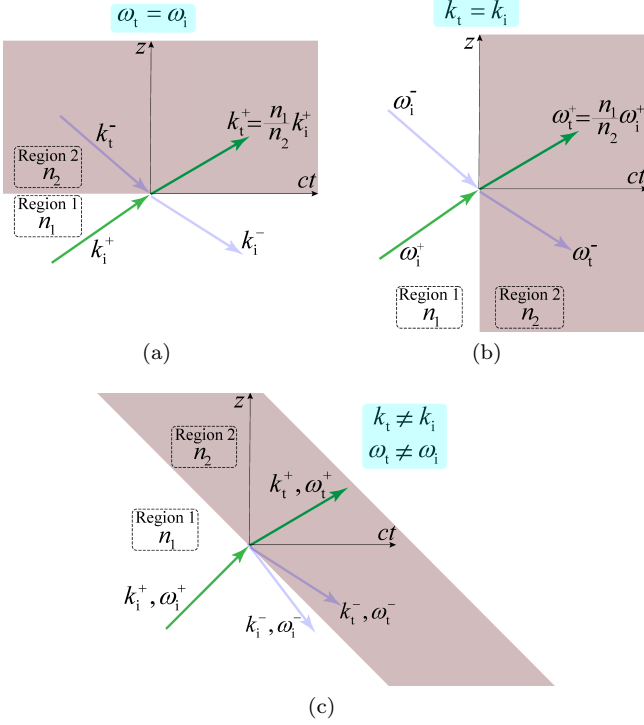


FIG. 2. Space-time diagrams showing scattering of forward and backward fields and conservation of energy and momentum for different scenarios. (a) Spatial interface, i.e., $n(z < 0) = n_1$ and $n(z > 0) = n_2$. (b) Temporal interface, i.e., $n(t < 0) = n_1$ and $n(t > 0) = n_2$. (c) Spatial-temporal interface, i.e., $n(z/c + t < 0) = n_1$ and $n(z/c + t > 0) = n_2$.

polarized electric field, with temporal frequency ω_0 and under an angle of incidence θ_i with respect to the normal of the grating, i.e.,

$$\mathbf{E}_i(x, z, t) = \hat{\mathbf{y}} E_0 e^{i(k_{x,i}x + k_{z,i}z - \omega_0 t)}, \quad (2)$$

where E_0 is the amplitude of the incident wave. In Eq. (2), $k_{x,i} = k_0 \sin(\theta_i) = \omega_0 \sin(\theta_i)/v_r$ and $k_{z,i} = k_0 \cos(\theta_i)$ are the x and z components of the incident wavevector, respectively.

The x component of the wavevector outside the STP grating, in region 3, reads

$$k''_{x,mn} = k''_n \sin(\theta''_{mn}), \quad (3)$$

where

$$k''_n = k''_0 + n \frac{\Omega}{v''_r}, \quad (4)$$

and where $k''_0 = \omega_0/v''_r$. The corresponding z component of the wavevector in region 3 is calculated using the Helmholtz relation, as

$$k''_{z,mn} = \sqrt{(k''_{mn})^2 - (k''_{x,mn})^2} = k''_n \cos(\theta''_{mn}). \quad (5)$$

The x and z components of the wavevector in region 1 ($k_{x,mn}$ and $k_{z,mn}$) and inside the grating ($k'_{x,mn}$ and $k'_{z,mn}$) can be achieved following the same procedure as in Eqs. (4) and (5). The space-time diffraction process may be simply interpreted as follows. The incident wave is refracted into the grating medium at $z = 0$, while generating an infinite set of time harmonics inside the grating, with frequencies $\omega_n = \omega_0 + n\Omega$ corresponding to the wavevectors $k'_n = k'_0 + n\Omega/v'_r$. The refracted space-time plane waves in the grating are diffracted into an infinite set of plane waves traveling toward the $z = d$ boundary. The space-time harmonic waves inside the grating are phase matched into propagating and evanescent waves in region 3, i.e., the x components of the wavevectors of the m th mode in regions 1 and 3 and the x component of the wavevector of the m th space-time harmonic field in region 2 must be the same.

To determine the spatial and temporal frequencies of the diffracted orders, we consider the momentum conservation law, i.e.,

$$k_{x,\text{diff}} = k_{x,\text{inc}} + mK, \quad (6a)$$

or

$$k''_{x,mn} = k_{x,mn} = k_{x,i} + mK, \quad (6b)$$

and the energy conservation law, i.e.,

$$\omega_{\text{diff}} = \omega_{\text{inc}} + n\Omega, \quad (6c)$$

or

$$\omega_n = \omega_0 + n\Omega, \quad (6d)$$

where $k_{x,\text{diff}}$ and $k_{x,\text{inc}}$ denote the x components of the wavevector of the diffracted and incident fields, respectively, and ω_{diff} and ω_{inc} represent the temporal frequencies of the diffracted and incident fields, respectively. Equation (6b), using (4), may be written as

$$\left(k''_0 + n \frac{\Omega}{v''_r}\right) \sin(\theta''_{mn}) = k_0 \sin(\theta_i) + mK, \quad (7)$$

where $k_0 = n_1 \omega_0/c$. Seeking for the angle of diffraction for the forward spatial-temporal diffracted orders in region 3, i.e., the m th spatial and n th temporal harmonic, yields

$$\sin(\theta''_{mn}) = \frac{n_1 \sin(\theta_i) + mK/k_0}{n_3 + n\Omega/\omega_0}, \quad (8)$$

The corresponding angle of diffraction for the backward diffracted orders in region 1 reads

$$\sin(\theta_{mn}) = \frac{\sin(\theta_i) + mK/k_0}{1 + n\Omega/\omega_0} \quad (9)$$

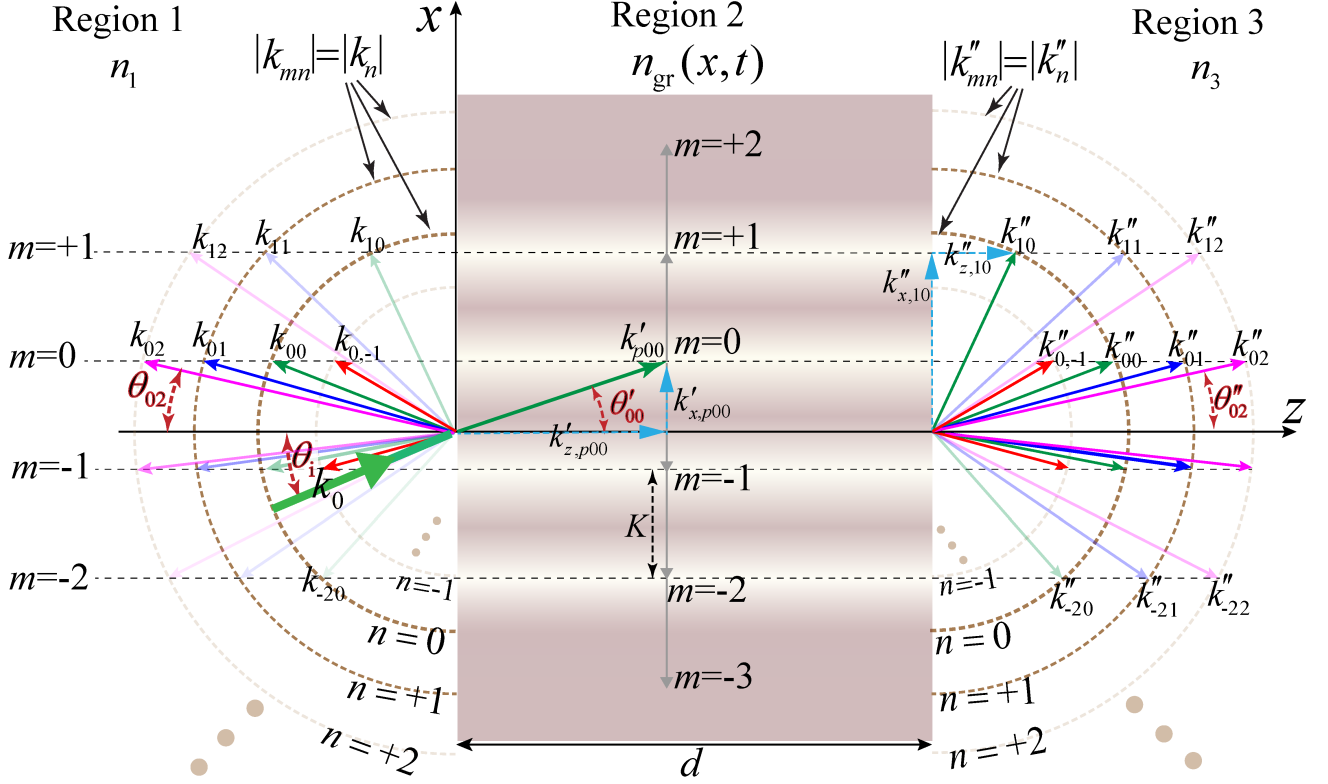


FIG. 3. Wavevector isofrequency diagram for the diffraction from a STP diffraction grating, exhibiting phase matching of spatial-temporal harmonic components of total field inside the grating with propagating backward diffracted orders in region 1, and forward diffracted orders in region 3. The diffracted spatial-temporal harmonics corresponding to $-1 < m < +2$ are propagating diffracted orders, whereas the harmonics corresponding to $m < -1$ and $m > +2$ are evanescent (cut off) outside the STP grating.

C. Propagating and evanescent Orders

For a given set of incident angles, spatial and temporal frequencies of the grating, and the wavelength of the incident beam, the grating equation in Eq. (6b) may be satisfied for more than one value of m and n . However, there exists a solution only when $|\sin(\theta_{mn})| < 1$. Diffraction orders corresponding to m and n satisfying this condition are called *propagating* orders. The other orders yielding $|\sin(\theta_{mn})| > 1$ correspond to imaginary z components of the wavevector $k_{z,mn}$ as well as complex angles of diffraction $\sin(\theta_{mn})$. These evanescent orders decrease exponentially with the distance from the grating, and hence, can be detected only at a distance less than a few wavelengths from the grating. However, these evanescent orders play a key role in some surface-enhanced grating properties and are taken into account in the theory of gratings. Evanescent orders are essential in some special applications, such as for instance waveguide and fiber gratings. The specular order ($m = 0$) is always propagating while the others can be either propagating or evanescent. The modulations with $2\pi/K \ll \lambda_0$ will produce evanescent orders for $m \neq 0$, while the modulations with $2\pi/K \gg \lambda_0$ will yield a large number of

propagating orders.

In the homogeneous regions, i.e., regions 1 and 3, the magnitude of the wavevectors of the backward- and forward-diffracted orders read

$$|k_{mn}| = |k_n|, \quad \text{and} \quad |k''_{mn}| = |k''_n| \quad (10)$$

As explained before, the x components of the diffracted wavevectors, $k_{x,mn}$ and $k''_{x,mn}$, can be deduced from the phase-matching requirements. Then, the propagating and evanescent nature of the corresponding orders will be specified based on the $k_{z,mn}$ and $k''_{z,mn}$, as follows. The real $k_{z,mn}$ s and $k''_{z,mn}$ s correspond to propagating orders, whereas the imaginary $k_{z,mn}$ s and $k''_{z,mn}$ s correspond to evanescent orders. The propagating and evanescent m th fields in regions 1 and 3 are shown in Fig. 3. The wavevectors in regions 1 and 3 possess magnitudes $|k_n|$ and $|k''_n|$, respectively. Hence, all the spatial diffraction orders for the n th temporal harmonic in these two regions share the same amplitude, i.e., $|k_{mn}| = |k_n|$ and $|k''_{mn}| = |k''_n|$. Semicircles with these radii are sketched in Fig. 3. The allowed wavevectors in these regions must be phased matched to the boundary components of the spatial-temporal diffracted order inside the grating. This is shown by the horizontal dashed lines in the figure. In

the qualitative illustration in Fig. 3, for the incident wave of wavevector k_0 and the grating with grating wavevector K and temporal frequency Ω , the $m = -1$ to $+2$ waves exist as propagating diffracted orders in regions 1 and 3. However, $m \leq -2$ and $m \geq +1$ will be diffracted as evanescent orders.

D. Diffracted Electromagnetic fields

The electromagnetic wave propagation and diffraction in general periodic media may be studied by several approaches. Among the proposed approaches, the modal approach [3, 9, 26, 66] and the coupled-wave approach [11, 24] represent the most common and insightful approaches for analysis of periodic media diffraction gratings, both of which provide exact formulations without approximations. Here, we study the wave diffraction inside the STP grating using the modal approach. The modal approach has also been referred to as the Bloch-Floquet (or Floquet-Bloch), characteristic-mode, and eigenmode approach. Such an approach expresses the electromagnetic fields inside the grating as a combination of an infinite number of modes, each of those individually satisfying Maxwell's equations.

First, we expand the field inside the modulated medium in terms of the spatial-temporal diffracted orders (m and n) of the field in the periodic structure. This is due to the fact that the electromagnetic waves in periodic media take on the same periodicity as their host. These spatial-temporal diffracted orders inside the grating are phase matched to diffracted orders (either propagating or evanescent) outside of the grating. The partial space-time harmonic fields may be considered as inhomogeneous plane waves with a varying amplitude along the planar phase front. These inhomogeneous plane waves are dependent and they exchange energy back and forth between each other in the modulated grating.

Since the electric permittivity of the grating is periodic in both space and time, with spatial frequency K and temporal frequency Ω , it may be expressed in terms of the double Fourier series expansion, as

$$n_{\text{gr}}^2(x, t) = \sum_m \sum_n \epsilon_{mn} e^{i(mKx - n\Omega t)}, \quad (11)$$

where ϵ_{mn} are complex coefficients of the permittivity, and K and Ω are the spatial and modulation frequencies, respectively. The electric field inside the grating is expressed in terms of a sum of an infinite number of modes, i.e.,

$$\mathbf{E}_2(x, z, t) = \sum_{p=-\infty}^{\infty} \mathbf{E}_{2,p}(x, z, t), \quad (12)$$

Given the spatial-temporal periodicity of the grating, the corresponding electric field of the p th mode inside the

grating may be decomposed into spatiotemporal Bloch-Floquet plane waves, as

$$\mathbf{E}_{2,p}(x, z, t) = \hat{\mathbf{y}} \sum_m \sum_n E'_{pmn} e^{i(k'_{x,pmn}x + k'_{z,pmn}z - \omega_n t)}, \quad (13)$$

where

$$k'_{x,pmn} = k'_{x,p0n} + mK = \left(k'_{p00} + n \frac{\Omega}{v'_r} \right) \sin(\theta'_{p0n}) + mK \quad (14)$$

and

$$k'_{z,pmn} = k'_{pmn} \cos(\theta_1), \quad (15)$$

In Eq. (14), θ'_{p0n} reads

$$\theta'_{p0n} = \tan^{-1} \left(\frac{k'_{x,p0n}}{k'_{z,p0n}} \right) \quad (16)$$

The corresponding magnetic field inside the grating reads

$$\begin{aligned} \mathbf{H}_2(x, z, t) &= \frac{1}{\eta} \hat{\mathbf{k}}'_{pmn} \times \mathbf{E}_2(x, z, t) \\ &= \sum_{p,m,n} \left(-\hat{\mathbf{x}} \frac{k'_{z,pmn}}{k'_{pmn}} + \hat{\mathbf{z}} \frac{k'_{x,pmn}}{k'_{pmn}} \right) \frac{E'_{pmn}}{\eta'} e^{i(k'_{x,pmn}x + k'_{z,pmn}z - \omega_n t)} \end{aligned} \quad (17)$$

The unknown field coefficients E'_{pmn} and $k'_{x,p00}$ are to be found through satisfying Maxwell's equations, that is,

$$\nabla \times \mathbf{E}_2(x, z, t) = -\frac{\partial \mathbf{B}_2(x, z, t)}{\partial t} \quad (18a)$$

$$\nabla \times \mathbf{H}_2(x, z, t) = \frac{\partial \mathbf{D}_2(x, z, t)}{\partial t} \quad (18b)$$

The corresponding wave equation for the STP grating may be derived from Eqs. (18a) and (18b) and reads

$$\nabla^2 \mathbf{E}_2(x, z, t) = \frac{1}{c^2} \frac{\partial^2}{\partial t^2} [\epsilon_{\text{gr}}(x, t) \mathbf{E}_2(x, z, t)] \quad (19)$$

We assume that the grating is invariant in the y direction (i.e., $\partial/\partial y = 0$). Then, inserting (12) into (19) yields

$$\begin{aligned} &\left(\frac{\partial^2}{\partial x^2} + \frac{\partial^2}{\partial z^2} \right) E'_{pmn} e^{i(k'_{x,pmn}x + k'_{z,pmn}z - \omega_n t)} \\ &= \frac{1}{c^2} \frac{\partial^2}{\partial t^2} \left(\sum_j \sum_q \epsilon_{jq} E'_{pmn} e^{i([k'_{x,pmn} + jK]x + k'_{z,pmn}z - [\omega_n + q\Omega]t)} \right) \\ &= \frac{1}{c^2} \frac{\partial^2}{\partial t^2} \sum_j \sum_q \epsilon_{m-j, n-q} E'_{pj q} e^{i(k'_{x,pmn}x + k'_{z,pmn}z - \omega_n t)} \end{aligned} \quad (20)$$

Solving Eq. 20 for the unknown field coefficients E'_{pmn} gives

$$E'_{pmn} = \frac{(\omega_n/c)^2}{(k'_{x,pmn})^2 + (k'_{z,pmn})^2} \sum_j \sum_q \epsilon_{m-j,n-q} E'_{pqj} \quad (21)$$

Next, we determine the backward diffracted fields in region 1 and forward diffracted fields in region 3. As depicted in Fig. 3, one must consider the multiple backward and forward-propagating diffracted orders that exist inside and outside of the grating. The total electric field in region 1 is the sum of the incident and the backward-traveling diffracted orders, as

$$\mathbf{E}_1 = \hat{\mathbf{y}} E_0 e^{i(k_{x,i}x + k_{z,i}z - \omega_0 t)} + \hat{\mathbf{y}} \sum_{m,n} E_{mn}^R e^{i(k_{x,mn}x - k_{z,mn}z - \omega_n t)} \quad (22)$$

where E_{mn}^R is the unknown amplitude of the m th reflected spatial-temporal diffracted orders in region 1, with the wavevectors $k_{x,mn}$ and $k_{z,mn}$. The total electric field in region 3 reads

$$\mathbf{E}_3 = \hat{\mathbf{y}} \sum_{m,n} E_{mn}^T e^{i(k''_{x,mn}x + k''_{z,mn}z - \omega_n t)}, \quad (23)$$

where E_{mn}^T is the amplitude of the m th transmitted spatial-temporal diffracted order in region 3, with the wavevectors $k''_{x,mn}$ and $k''_{z,mn}$. To determine the unknown field coefficients of the backward and forward diffracted orders, E_{mn}^R and E_{mn}^T , we enforce the continuity of the tangential electric and magnetic fields at the boundaries of the grating at $z = 0$ and $z = d$. The electric field continuity condition between regions 1 and 2 at $z = 0$, $E_{1y}(x, 0, t) = E_{2y}(x, 0, t)$, using (12) and (22), reduces to

$$\delta_{n0} E_0 e^{ik_{x,i}x} + \sum_{m,n} E_{mn}^R e^{ik_{x,mn}x} = \sum_{p,m,n} E'_{pmn} e^{ik'_{x,pmn}x}, \quad (24)$$

and the corresponding magnetic field continuity condition, i.e., $H_{1x}(x, 0, t) = H_{2x}(x, 0, t)$, may be formulated as

$$\begin{aligned} & \cos(\theta_i) \delta_{n0} \delta_{n0} E_0 e^{ik_{x,i}x} - \cos(\theta_{mn}) E_{mn}^R e^{ik_{x,mn}x} \\ &= \eta_1 \sum_p \frac{k'_{z,pmn}}{k'_{p,pmn}} \frac{E'_{pmn}}{\eta'} e^{ik'_{x,pmn}x}, \end{aligned} \quad (25)$$

The electric field continuity condition between regions 2 and 3 at $z = d$, $E_{2y}(x, d, t) = E_{3y}(x, d, t)$, reduces to

$$E_{mn}^T = \sum_p E'_{pmn} e^{i([k'_{x,pmn} - k''_{x,mn}]x + [k'_{z,pmn} - k''_{z,mn}]d)}, \quad (26)$$

while the corresponding tangential magnetic field continuity condition between regions 2 and 3 at $z = d$,

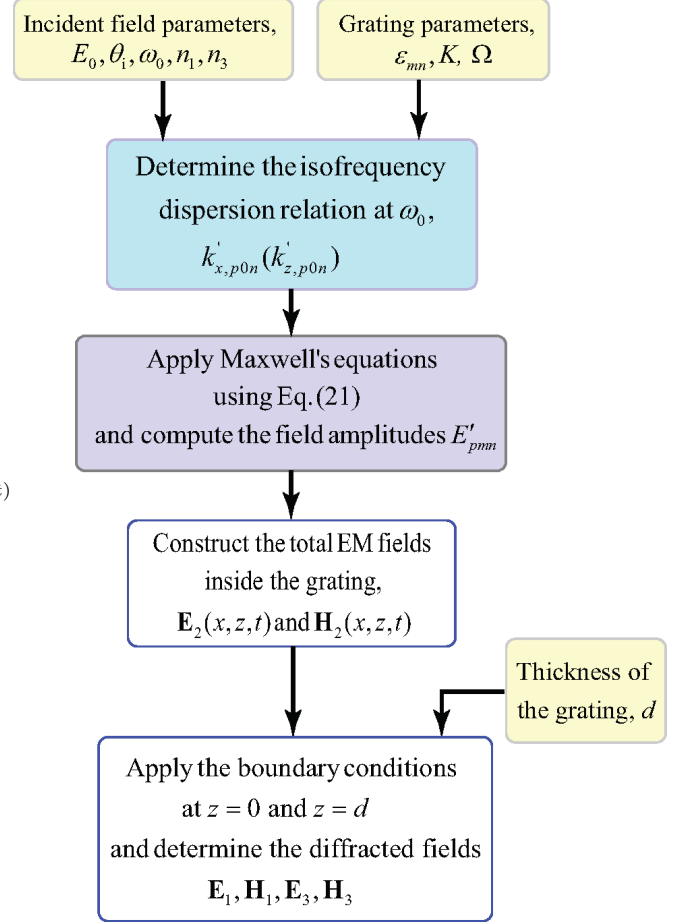


FIG. 4. Procedure for deriving the scattered electromagnetic fields inside and outside of a STP grating.

$H_{2x}(x, d, t) = H_{3x}(x, d, t)$, reads

$$\sum_p \frac{E'_{pmn}}{\eta'} e^{i([k'_{x,pmn} - k''_{x,mn}]x + [k'_{z,pmn} - k''_{z,mn}]d)} \quad (27)$$

$$= \frac{\cos(\theta_{mn})}{\cos(\theta_i)} \frac{E_{mn}^T}{\eta''}$$

Solving the above four equations, i.e., Eqs. (24)- (27), together provides the four unknown field amplitudes, i.e., the forward and backward field amplitudes inside the grating ($E_{pmn}^{'+}$ and $E_{pmn}^{'-}$), and the reflected and transmitted field amplitudes outside the grating (E_{mn}^R and E_{mn}^T). Figure 4 overviews the procedure for determining unknown field amplitudes and the dispersion relation of a STP grating.

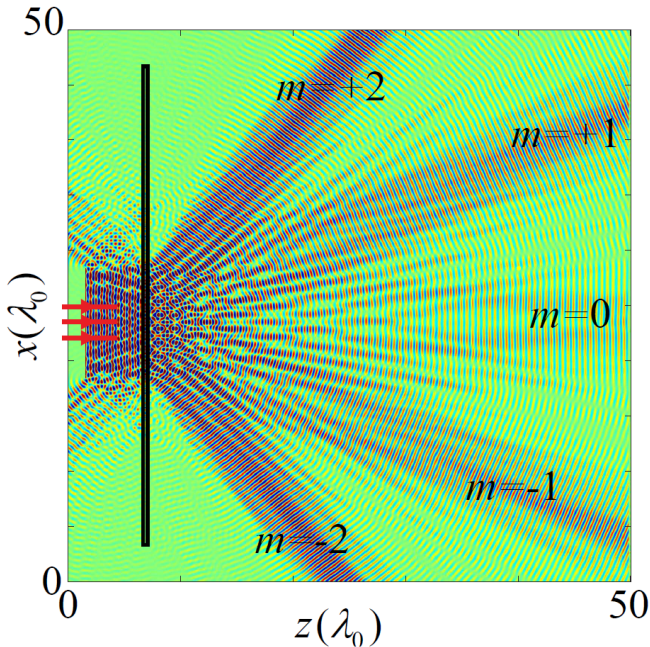


FIG. 5. FDTD numerical simulation results of the y -component of the electric field for the diffraction from a conventional spatially periodic time-independent grating ($\Omega = 0$), with $\theta_i = 0^\circ$, $\omega_0 = 2\pi \times 10$ GHz, $\delta_\epsilon = 0.5$, $K = 0.4k_0$, $d = 0.8\lambda_0$.

III. ILLUSTRATIVE EXAMPLES

A. Conventional spatially periodic static diffraction grating

For the sake of comparison, we first investigate the diffraction from a conventional planar spatially periodic (static) diffraction gratings [1, 3, 9, 10]. Such a static grating assumes a sinusoidal relative electric permittivity in the region from $z = 0$ to $z = d$ given by

$$n_{\text{gr}}^2(x) = \epsilon_{\text{av}} + \delta_\epsilon [1 + \sin(Kx)], \quad (28)$$

and interfaced with two semi-infinite dielectric regions, characterized with refractive indices n_1 and n_3 , respectively. Figure 5 shows the time domain FDTD simulation results for the diffraction from a conventional spatially periodic grating with $\theta_i = 0^\circ$, $\omega_0 = 2\pi \times 10$ GHz, $\delta_\epsilon = 0.5$, $\Omega = 0$, $K = 0.4k_0$, $d = 0.8\lambda_0$. It may be seen from this figure that, for a monochromatic incident wave, all spatial diffracted orders possess the same wavelength (frequency). Another observed phenomenon is that, since the grating is "unidirectional", the diffraction pattern for a normal incidence ($\theta_i = 0$) is symmetric with respect to the x axis. Table I lists the analytical results, derived from (8), for the diffraction angles θ_m (in degrees) of the conventional transmissive space periodic diffraction grating in Fig. 1(a).

TABLE I. Analytical results for the diffraction angles θ_m (in degrees) of the transmissive conventional spatially periodic time-independent grating ($\Omega = 0$), corresponding to the FDTD numerical simulation results in Fig. 5.

m						
-3	-2	-1	0	+1	+2	+3
Ev.	-53.1	-23.58	0	23.58	53.1	Ev.

B. Transmissive STP diffraction grating

Next, we demonstrate the diffraction from a planar STP (dynamic) diffraction grating. As a particular case, which is practical and common, we study the grating with a sinusoidal relative electric permittivity in the region from $z = 0$ to $z = d$ given by

$$n_{\text{gr}}^2(x, t) = \epsilon_{\text{av}} + \delta_\epsilon [1 + \sin(Kx - \Omega t)]. \quad (29)$$

To compute the solution derived in Sec. IID, we shall write the expression in (29) in terms of its spatial-temporal Fourier components, considering the general form given in Eq. (11), i.e.,

$$n_{\text{gr}}^2(x, t) = \epsilon_{-1,-1} e^{-j(Kx - \Omega t)} + \epsilon_{00} + \epsilon_{11} e^{+j(Kx - \Omega t)}, \quad (30a)$$

with

$$\epsilon_{11} = -\epsilon_{-1,-1} = \delta_\epsilon / 2i \quad \text{and} \quad \epsilon_{00} = \epsilon_{\text{av}} + \delta_\epsilon. \quad (30b)$$

We next insert the nonzero terms of the permittivity, given in (30b), into Eq. (21), and determine the electromagnetic fields inside the grating, dispersion relation [26, 27, 31], and the diffracted fields. Table II lists the analytical results for the diffraction angles θ_{mn} (in degrees) of the transmissive STP diffraction grating, for normal incidence of a monochromatic wave, $\theta_i = 0^\circ$, $\omega_i = \omega_0 = 2\pi \times 10$ GHz, where $\delta_\epsilon = 0.5$, $\Omega = 0.28\omega_0$, $K = 0.4k_0$, $d = 0.8\lambda_0$.

Figure 6(a) shows the corresponding time domain FDTD simulation results for the diffraction from this STP grating. We observe from this figure that, in contrast with the conventional case in Fig. 5, the diffraction pattern of the STP grating is asymmetric with respect to the x axis. The second observed phenomenon, as expected, is that the diffracted orders possess different wavelengths, which correspond to different frequencies. From Fig. 6(a), one may conclude that each diffracted order is attributed to a single frequency. However, this is not true. To see the exact phenomenon, we shall look at the frequency spectrum of the diffracted orders, by performing a fast Fourier transform of the transmitted diffracted orders at different angles. Figures 6(b) to 6(g) plot the analytical and FDTD numerical simulation frequency domain responses for the $m = -1$ to $m = +4$ diffracted orders, corresponding to the analytical results listed in Tab. II. These figures show that each diffracted spatial order includes an infinite set of temporal harmonics, $\omega_n = \omega_0 + n\Omega$, with n being any integers.

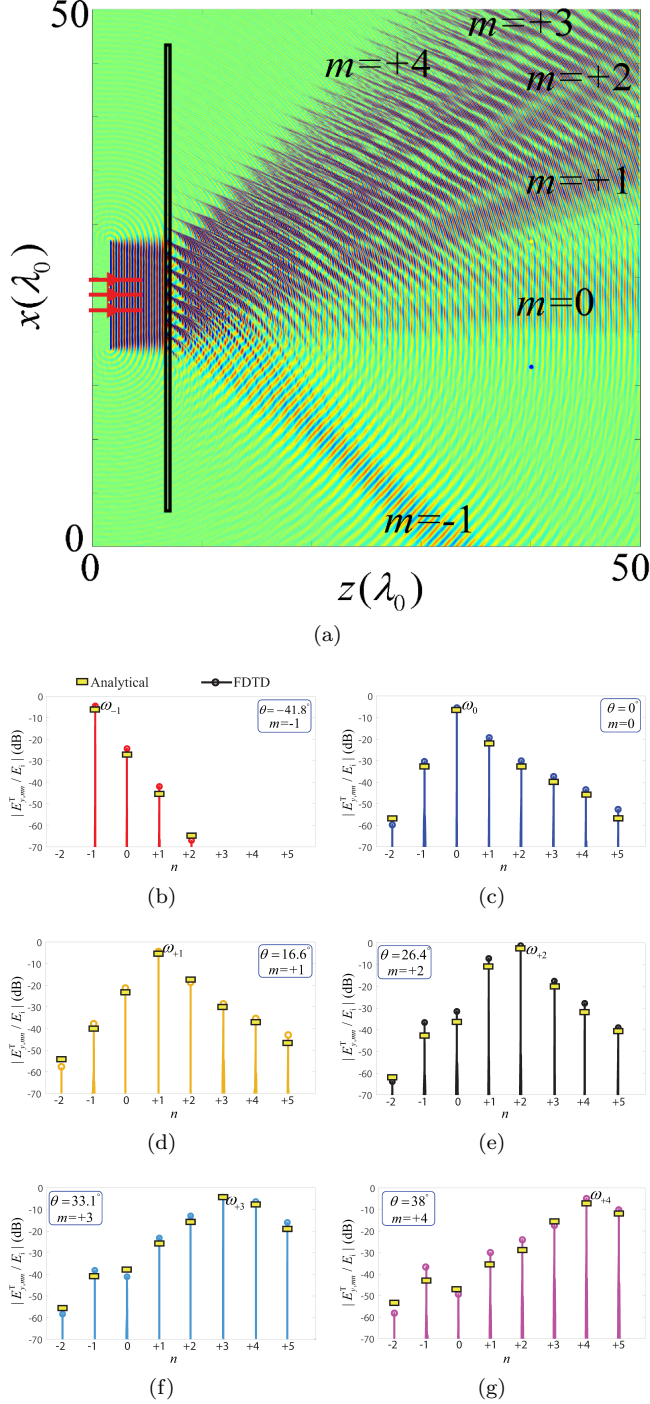


FIG. 6. Analytical and FDTD simulation results for the spatial-temporal diffraction from a STP grating, for normal incidence of a plane wave ($\theta_i = 0^\circ$) with temporal frequency $\omega_0 = 2\pi \times 10$ GHz, where $\delta_\epsilon = 0.5$, $\Omega = 0.28\omega_0$, $K = 0.4k_0$, $d = 0.8\lambda_0$. (a) FDTD simulation time domain response of the y -component of the transmitted electric field, i.e., $E_{y,mn}^T$. (b)-(g) Frequency domain response for (b) $m = -1$. (c) $m = 0$. (d) $m = +1$. (e) $m = +2$. (f) $m = +3$. (g) $m = +4$. The analytical results for the angles of diffraction are listed in Table II.

TABLE II. Analytical results for diffraction angles θ_{mn} (in degrees) of the transmissive STP diffraction grating, where the FDTD numerical simulation results are given in Fig. 6.

	m						
	-3	-2	-1	0	+1	+2	+3
$n = -3$	Ev.	Ev.	Ev.	0	Ev.	Ev.	Ev.
$n = -2$	Ev.	Ev.	-65.4	0	65.4	Ev.	Ev.
$n = -1$	Ev.	Ev.	-33.7	0	33.7	Ev.	Ev.
$n = 0$	-70	-38.7	-18.2	0	18.2	38.7	70
$n = +1$	-59	-34.85	-16.6	0	16.6	34.85	59
$n = +2$	-50.3	-30.8	-14.86	0	14.86	30.8	50.3
$n = +3$	-40.77	-25.8	-12.55	0	12.55	25.8	40.7

C. Effect of the grating thickness

It is of great interest to investigate the effect of the thickness of the STP grating (d) on the generation of space and time diffraction orders and the grating efficiency. In general, diffraction gratings may be classified in two main categories, i.e., *thin* and *thick* gratings, each of which exhibiting its own angular and wavelength selectivity characteristics. The thin gratings usually result in Raman-Nath regime diffraction, where multiple diffracted orders are produced. In contrast, the thick gratings usually result in Bragg regime diffraction, where only one single diffracted order is produced. Following the procedure described in [3, 12], we characterize these two diffraction regimes, i.e., the Bragg and Raman-Nath regimes, by the dimensionless parameter

$$Q_n = \frac{v_r K^2 d}{(\omega_0 + n\Omega) \cos(\theta'_n)} \quad (31)$$

The grating strength parameter is represented by

$$\gamma_n = \frac{\delta_\epsilon}{\epsilon_{av}} \frac{d(\omega_0 + n\Omega)}{4v_r \cos(\theta'_n)} \quad (32)$$

for TE polarization, and

$$\gamma_n = \frac{\delta_\epsilon}{\epsilon_{av}} \frac{d(\omega_0 + n\Omega) \cos(2\theta'_n)}{4v_r \cos(\theta'_n)} \quad (33)$$

for TM polarization.

1. Thin STP grating (RamanNath regime)

The required condition for thin STP gratings exhibiting Raman-Nath regime diffraction is represented by

$$Q_n \gamma_n \leq 1 \quad (34)$$

Thin gratings may be also characterized as gratings showing small angular and wavelength selectivity. As the incident wave is dephased (either in angle of incidence or in wavelength) from the Bragg condition, the diffraction

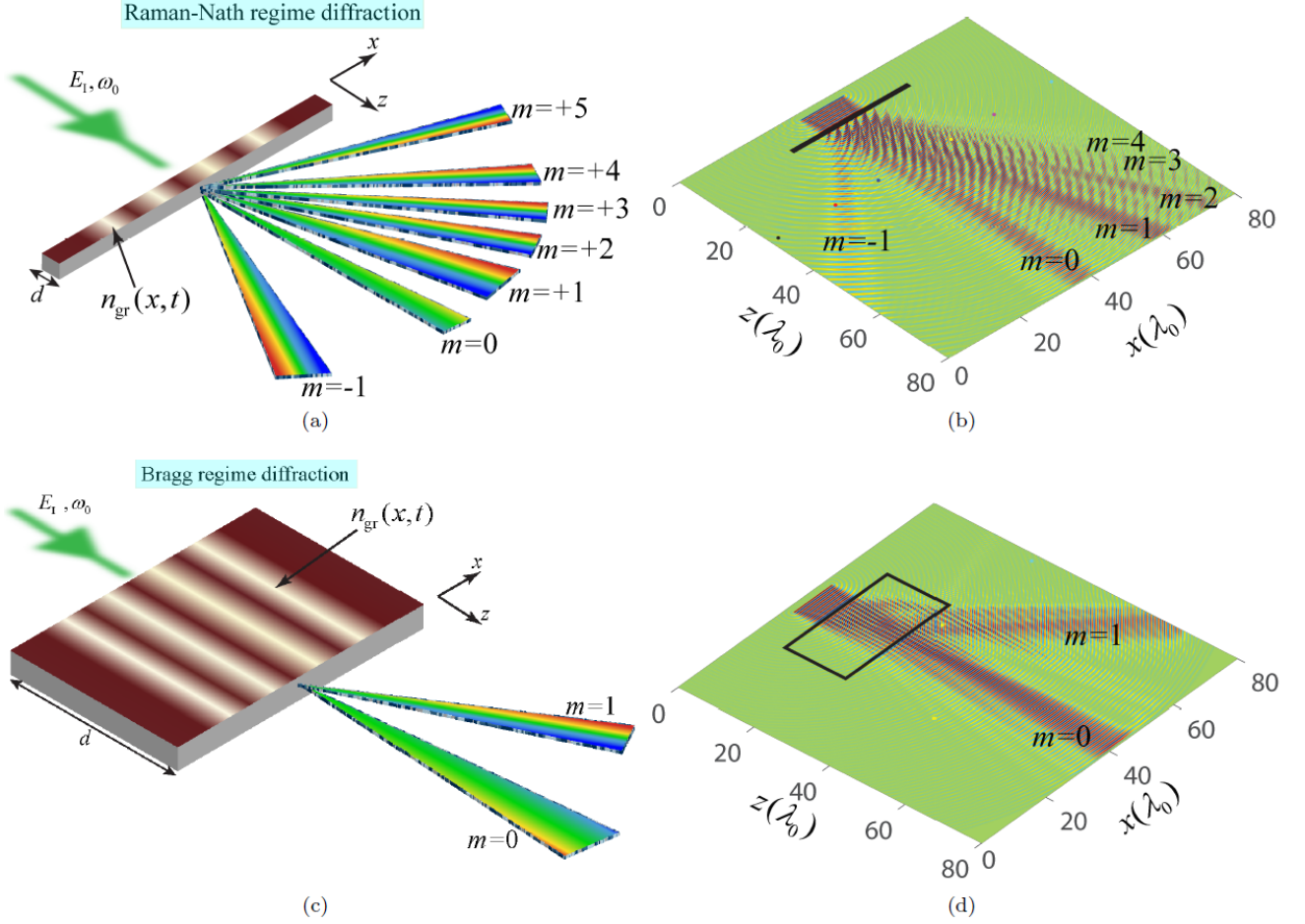


FIG. 7. Operation regimes of STP transmissive diffraction gratings, for normal incidence ($\theta_i = 0^\circ$), $\omega_0 = 2\pi \times 10$ GHz. (a) Raman-Nath regime diffraction of a thin grating, where $\Omega = 0.4\omega_0$ and $K = 0.4k_0$, $\delta_\epsilon = 0.5$ and $d = 0.5\lambda$. (b) Bragg regime diffraction of a thick grating, where $\Omega = 0.347\omega_0$ and $K = 0.867k_0$, $\delta_\epsilon = 0.1$ and $d = 16\lambda$.

efficiency decreases. The angular range or wavelength range for which the diffraction efficiency decreases to half of its on-Bragg-angle value is determined by the thickness of the grating d expressed as a number of grating periods $\Lambda = 2\pi/K$. For a thin grating this number is reasonably chosen to be

$$Kd \leq 20\pi \quad (35)$$

Figure 7(a) shows a generic representation of the Raman-Nath regime diffraction in STP transmissive diffraction gratings, for normal incidence ($\theta_i = 0^\circ$), $\omega_0 = 2\pi \times 10$ GHz, $\Omega = 0.4\omega_0$ and $K = 0.4k_0$, $\delta_\epsilon = 0.5$ and $d = 0.5\lambda$. Figure 7(b) shows the numerical simulation results for Raman-Nath regime diffraction of the STP grating in Fig. 7(a). Following the procedure described in [3, 12] (for conventional spatially periodic gratings), for a thin transmissive STP grating operating in the Raman-Nath regime, the diffraction efficiency reads

$$\eta_{mn} = \frac{P_{mn}}{P_{\text{inc}}} = J_m^2(2\gamma_n) \quad (36)$$

where P_{mn} and P_{inc} are the diffracted and incident powers, respectively, and where J represents the, integer-order, ordinary Bessel function of the first kind.

2. Thick STP grating (Bragg regime)

The Bragg regime diffraction may be achieved in thick gratings, where then the required condition is

$$\frac{Q_n}{2\gamma_n} \geq 10 \quad (37)$$

Thick gratings are capable of exhibiting strong angular and wavelength selectivity. A relatively small change in the angle of incidence from the Bragg angle or a relatively small change in the wavelength at the Bragg angle may result in a relatively strong dephasing, which in turn, decreases the diffraction efficiency. Thick grating behavior occurs when

$$Kd \geq 20\pi \quad (38)$$

Figure 7(c) shows a generic representation of the Bragg regime diffraction in STP transmissive diffraction gratings, for normal incidence ($\theta_i = 0^\circ$), $\omega_0 = 2\pi \times 10$ GHz, $\Omega = 0.4\omega_0$ and $K = 0.4k_0$, $\delta_\epsilon = 0.5$ and $d = 0.5\lambda$. Figure 7(d) shows the numerical simulation results for Bragg regime diffraction of the STP grating in Fig. 7(c). Following the procedure described in [3, 12] (for conventional spatially periodic gratings), for a thick transmissive STP grating operating in the Bragg regime, the diffraction efficiency reads

$$\eta_{1n} = \sin^2(2\gamma_n) \quad (39)$$

IV. NONRECIPROCAL DIFFRACTION BY STP GRATINGS

A. Nonreciprocal Transmissive Diffraction

Over the past few years, there has been a surge of interest in the nonreciprocal wave transmission [24, 26, 27, 67–69]. Here, we show how a nonreciprocal wave diffraction may be achieved by a spatiotemporally periodic grating. The spatial diffraction of electromagnetic waves by natural media is reciprocal under reversal of the incident wave direction. However, asymmetric and nonreciprocal spatial diffraction of electromagnetic waves has been investigated, over the past two decades, in a few articles [70–74]. Here we elaborate on the nonreciprocal spatial-temporal diffraction provided by a STP grating that can be used for the realization of different communication and optical systems, such as tunable beam steering.

Figure 8(a) illustrates a particular example, where a $+z$ -propagating incident field (forward wave incidence) obliquely impinges on a STP grating. The STP grating possess an x -traveling space-time-varying permittivity $\epsilon(x, t) = \epsilon_{av} + \delta_\epsilon[1 + \sin(Kx - \Omega t)]$. Figure 8(b) shows the FDTD numerical simulation result of the transmissive diffraction by the STP diffraction grating in Fig. 8(a) with $\theta_i = 35^\circ$, $\omega_0 = 2\pi \times 10$ GHz, where $\delta_\epsilon = 0.5$, $\Omega = 2\pi \times 4$ GHz, $d = 0.8\lambda_0$. As expected, the diffracted spatial-temporal orders possess different wavelengths and different amplitudes. Now, we consider a $-z$ -propagating incident field (backward wave incidence) that obliquely impinges on the same STP grating as in Figs 8(a) and 8(b), but from the other side of the STP grating and under the same angle of incidence, i.e., $\theta_i = 35^\circ$. This scenario is depicted in Fig. 8(c), and the corresponding time domain response is shown in Fig. 8(d). Comparing the numerical simulation results in Figs. 8(b) and 8(d), we see that the STP grating introduces completely different diffraction patterns for forward and backward incidence. This includes, difference in the angle of diffraction and amplitude of the diffracted fields.

B. Nonreciprocal Reflective Diffraction

Here, we show the operation of the STP diffraction grating in the reflective mode. Such a grating may be realized based on the combination of a STP diffraction grating and a metallic surface. Metals naturally reflect light with high efficiency, so that by integrating a STP grating and a metal, one may achieve a fully reflective STP diffraction grating. Figure 9(a) depicts a reflective STP grating, where a perfect electric conductor (PEC) is used at the bottom of the structure providing full reflection of spatial-temporal diffractions. Figure 9(b) provides the numerical results for the diffraction by the grating in Fig. 9(a) for forward incidence, where $\theta_i = 35^\circ$, and with an $+x$ -traveling modulation, i.e., $\epsilon(x, t) = \epsilon_{av} + \delta_\epsilon[1 + \sin(Kx - \Omega t)]$, with $\omega_0 = 2\pi \times 10$ GHz, where $\delta_\epsilon = 0.5$, $\Omega = 2\pi \times 4$ GHz, $d = 0.8\lambda_0$. Following the same operation as the transmissive STP grating, here the diffracted orders possess different wavelengths.

Next, to investigate the nonreciprocity of the reflective STP grating, we consider incidence of the wave under the angle of incidence $\theta_i = -35^\circ$, as sketched in Fig. 9(c). The corresponding FDTD numerical simulation result is shown in Fig. 9(d). Comparing the results of the forward and backward incidence, provided in Figs. 9(b) and 9(d), respectively, one may obviously see that the reflective diffraction by the grating is nonreciprocal. Such a nonreciprocal reflective diffraction includes nonreciprocal angles of diffraction and nonreciprocal amplitudes of the diffracted fields. Figures 9(e) to 9(h) plot the FDTD numerical simulation frequency domain responses for the $m = -1$ to $m = +2$ diffracted orders. Figure 9(i) plots the isolation of each spatial-temporal diffracted order for forward and backward incidences shown in Figs. 9(b) and 9(d), respectively. Table III lists the analytical results for the diffraction angles θ_{mn} (in degrees) of the reflective STP diffraction grating, considering an incident field impinging on the surface of the grating under the incident angle of $\theta_i = 35^\circ$ for forward incidence and $\theta_i = -35^\circ$ for backward incidence.

V. PRACTICAL APPLICATIONS

The proposed STP grating offers unique properties that can be utilized for the realization of new types of electromagnetic devices and operations, such as for instance, nonreciprocal beam shaping and beam coding, multi-functionality antennas, tunable and nonreciprocal beam steering, enhanced resolution holography, multiple images holography, illusion cloaking, etc.

Figure 10 presents an original application of the STP diffraction grating to wireless communications. Such a communication system is hereby called space-time diffraction code multiple access (STDCMA) system. In the example provided in Fig. 10, we consider three pairs of transceivers (in practice one may consider more pairs of transceivers). In such a scenario, only the transceiver

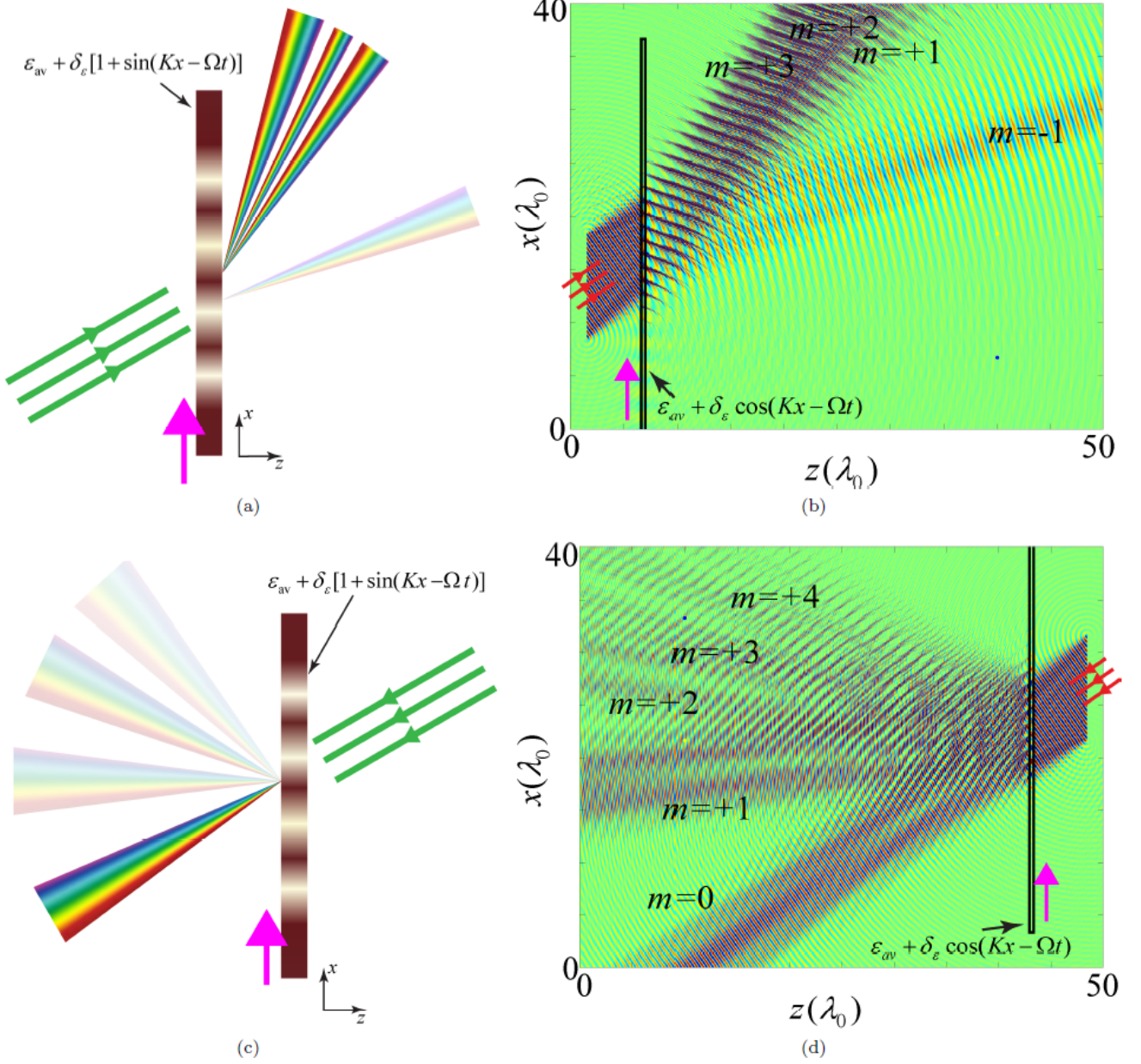


FIG. 8. Nonreciprocal wave diffraction from a transmissive STP grating with sinusoidal space-time-varying permittivity, i.e., $\epsilon(x, t) = \epsilon_{av} + \delta_\epsilon \sin(Kx - \Omega t)$, where $\theta_i = 35^\circ$, $\omega_0 = 2\pi \times 10$ GHz, $\delta_\epsilon = 0.5$, $\Omega = 2\pi \times 4$ GHz and $d = 0.8\lambda_0$. (a) and (b) Forward incidence. (c) and (d) Backward incidence.

pairs that share the same space-time diffraction pattern can communicate. Each diffraction pattern is attributed to the properties of the grating space-time modulation, i.e., the input frequency, where the input data (message) plays the role of the modulation signal. For a specified input data (modulation signal), a unique diffraction pattern is created. In the particular example in Fig. 10, the transceiver pairs that are allowed to communicate are 1 and 1', 2 and 2', and 3 and 3', so that the transceivers 2' and 3' (2 and 3) are incapable of retrieving the data sent by the transceiver 1 (1'), and the transceivers 1' and 3' (1 and 3) are incapable of retrieving the data sent by

the transceiver 2 (2'), and so forth. Each communication pair shares a certain space-time diffraction *pattern*. Each diffraction pattern can be created by certain space-time modulation parameters, e.g. δ_ϵ , ϵ_{av} , the K/Ω ratio, and the grating thickness d . Since the radiation pattern provided by a STP diffraction grating is very diverse and is very sensitive to the space-time modulation parameters, an optimal isolation between the transceivers can be achieved by proper design of the diffraction patterns.

Such a multiple access scheme is endowed with *full-duplex* operation, thanks to the unique nonreciprocity

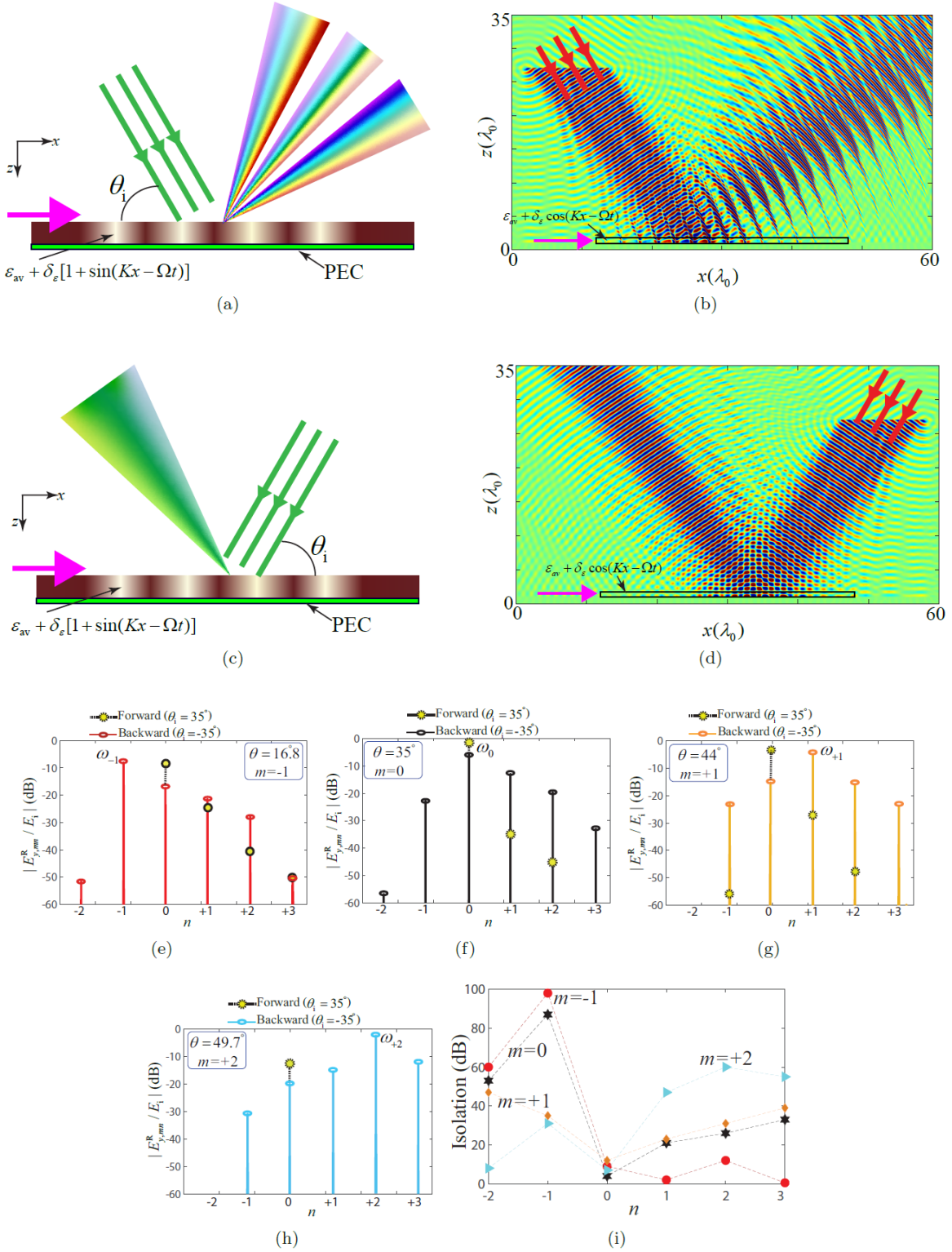


FIG. 9. FDTD numerical simulation results for a $+x$ -traveling modulation, i.e., $\epsilon(x, t) = \epsilon_{av} + \delta_\epsilon [1 + \sin(Kx - \Omega t)]$, with $\omega_0 = 2\pi \times 10$ GHz, where $\delta_\epsilon = 0.5$, $\Omega = 2\pi \times 4$ GHz, $d = 0.8\lambda_0$. (a) and (b) Forward incidence, where $\theta_i = 35^\circ$. (c) and (d) Backward incidence, where $\theta_i = -35^\circ$. (e)-(h) Frequency spectrum of the diffracted orders for forward ($\theta_i = 35^\circ$) and backward $\theta_i = -35^\circ$ incidences, exhibiting nonreciprocal diffraction. (i) Isolation between forward and backward diffracted orders achieved from the results in (e)-(h). The analytical results for the angle of diffraction are listed in Table III.

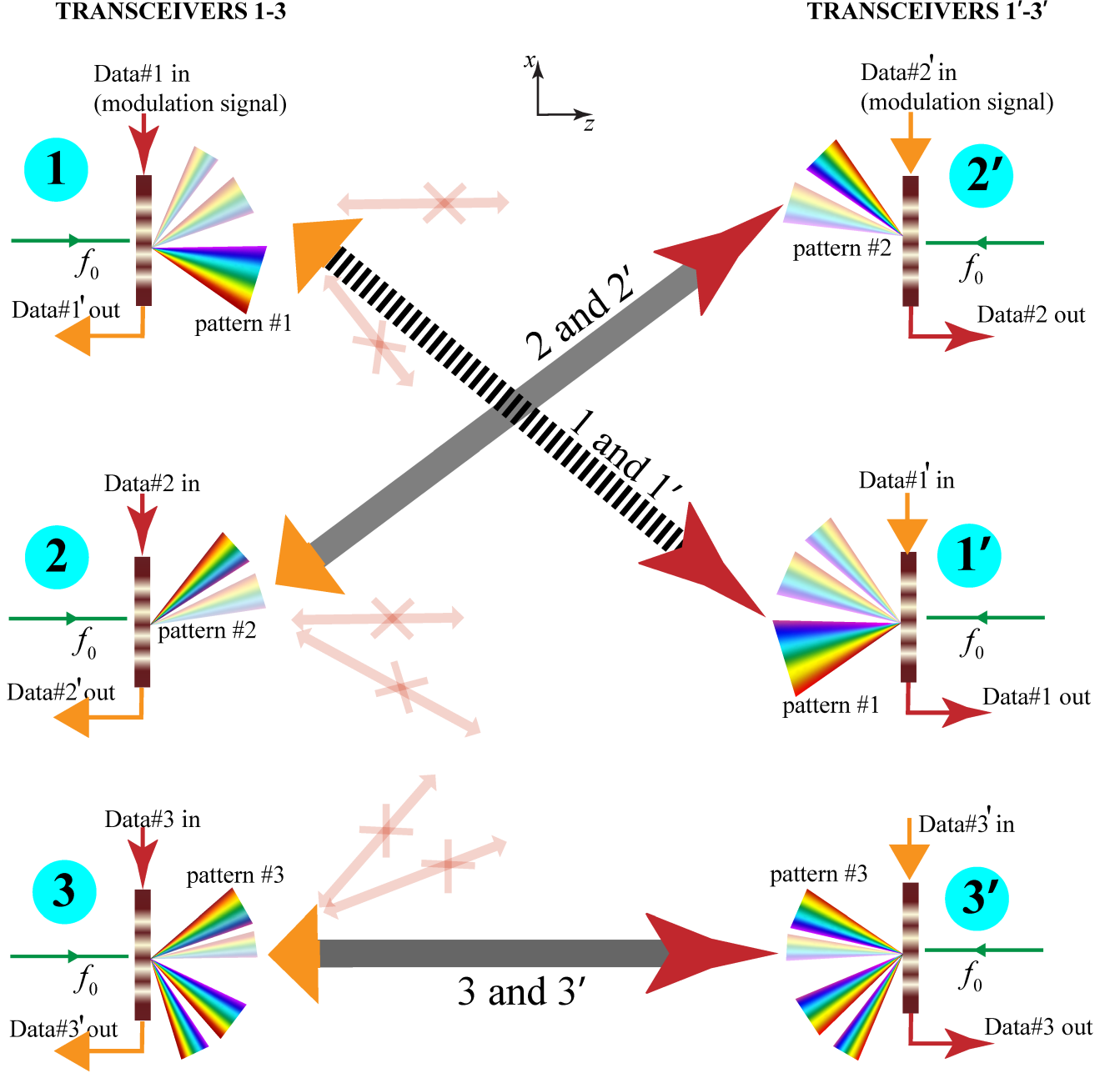


FIG. 10. Application of STP diffraction gratings to a full-duplex space-time diffraction code multiple access (STDCMA) system.

provided by the properties of a STP diffraction grating. Figure 11 depicts the architecture of a STP-diffraction-grating-based transceiver in the STDCMA system in Fig. 10. Such an architecture is composed of a STP diffraction grating illuminated by an incident wave with frequency f_0 . In the transmit mode (TX), the grating is modulated by the input data denoted by ψ_{TX} which is injected to the grating from the top and travels in the $-x$ direction. In the receive mode (RX), the incoming wave (which includes a set of spatial-temporal diffraction orders) impinges on the grating and while interacting with

the incident wave with frequency f_0 , yields a $-x$ traveling wave inside the grating, denoted by ψ_{RX} . We shall stress that traveling of the ψ_{RX} signal in the $-x$ direction is enforced by proper design of the grating, which will be explained later.

As we see in Fig. 11, the signal wave at the receiver port is composed of the received signal (ψ_{RX}) plus a portion of the input data of the transmission mode ($\alpha\psi_{TX}$). To ensure complete cancellation of the ψ_{TX} in the receiver port, we may use the circuit in the left side of Fig. 11. This circuit is composed of a signal splitter that

TABLE III. Analytical results for diffraction angles θ_{mn} (in degrees) of the reflective STP diffraction grating, where the FDTD numerical simulation results are given in Fig. 9.

	Incidence	-3	-2	m				
		-3	-2	-1	0	+1	+2	+3
$n = -3$	Forw.:	Ev.	Ev.	-60	Ev.	Ev.	Ev.	Ev.
	Backw.:	Ev.	Ev.	Ev.	Ev.	-60.2	Ev.	Ev.
$n = -2$	Forw.:	Ev.	Ev.	60	Ev.	Ev.	Ev.	Ev.
	Backw.:	Ev.	Ev.	Ev.	Ev.	60.2	Ev.	Ev.
$n = -1$	Forw.:	Ev.	-22.2	16.8	72.9	Ev.	Ev.	Ev.
	Backw.:	Ev.	Ev.	Ev.	73	16.8	-22.1	Ev.
$n = 0$	Forw.:	-38.8	-13.1	10	35	76.8	Ev.	Ev.
	Backw.:	Ev.	Ev.	76.8	35	10	-13	-38.8
$n = +1$	Forw.:	-26.6	-9.3	7.1	24.2	44	78.8	Ev.
	Backw.:	Ev.	78.8	44	24.2	7.1	-9.3	-26.6
$n = +2$	Forw.:	-20.4	-7.2	5.5	18.6	32.7	49.7	80.2
	Backw.:	80.2	49.7	32.7	18.6	5.5	-7.2	-20.4
$n = +3$	Forw.:	-16.5	-5.9	4.5	15.1	26.3	38.6	53.7
	Backw.:	53.7	38.6	26.3	15.1	4.5	-5.9	-16.5

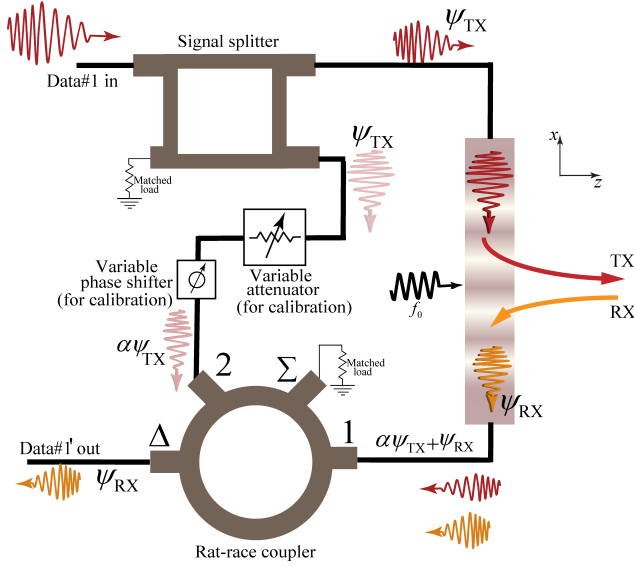


FIG. 11. Full-duplex operation of STP-diffraction-based transceivers in Fig. 10 based on unidirectional ($-x$ direction) traveling of both TX and RX signals, where complete cancellation of the TX signal in the RX port is enforced.

provides a sample from the input data of the transmit mode (ψ_{TX}), a variable attenuator and a variable phase shifter for calibration purposes to provide $\alpha\psi_{TX}$. Then, the signal wave at the receiver port, i.e., $\psi_{RX} + \alpha\psi_{TX}$, will be subtracted from the calibrated sample signal, that is $\alpha\psi_{TX}$, by a rat-race coupler. Thus, the signal at the difference port of the rat-race coupler is the desired received

signal ψ_{RX} . It is worth mentioning that the calibration of the architecture can be performed by disconnecting the RX port from port-1 of the rat-race coupler, connecting port-1 to a match load, and then seeking for a null at the difference port of the rat-race coupler by adjusting the variable attenuator and variable phase shifter, so that ψ_{TX} is completely canceled out at the difference port of the rat-race coupler.

An elegant feature of the transceiver scheme in Fig. 11 is that the diffraction grating is used as the receiver (as well as the transmitter), where the received signal wave acts as the modulation signal (specifies the K and Ω parameters) instead of the incident field. The key reason for the duplexing operation is that, inside the grating the wave can only flow downstream. Figure 12 shows how the full-duplex operation is achieved by proper design of the diffraction grating, where only negative diffraction orders, i.e., $-x$ propagating orders, are generated, while positive diffraction orders, that is $+x$ propagating orders, are evanescent. This way, we ensure that inside the grating, all the diffraction orders are traveling in the $-x$ direction, in both the transmit and receive modes. In Fig. 12, transceiver 1 operates in the transmit mode, where the input data (ψ_{TX}) is injected to the grating from the top and while interacting with the incident wave with the wavenumber k_0 , generates a number of nonpositive diffraction orders, i.e., $m \geq 0$. In the right side of Fig. 12, transceiver 1' receives the diffracted orders by transceiver 1, so that the resultant wave inside ψ_{RX} exits the grating from the bottom port of the grating, as all the diffraction orders can only travel in the $-x$ direction.

VI. CONCLUSION

We have presented the analysis and characterization of space-time periodic (STP) diffraction gratings as the generalized version of conventional spatially periodic diffraction gratings. Such STP gratings offer enhanced functionalities and exotic behaviour. It is shown that such gratings provide an asymmetric diffraction pattern, non-reciprocal diffraction, and enhanced diffraction efficiency as well as frequency generation. Moreover, each spatial diffraction order includes an infinite set of temporal diffraction orders. We provided the theoretical investigation of the problem, which has been supported by FDTD numerical simulation results. Such structures with marked differences with conventional spatially periodic diffraction gratings are expected to find interesting applications in optical and communication systems. As a particular example, we have proposed the space-time diffraction code multiple access (STDCMA) system, as a promising communication system featuring full-duplex operation.

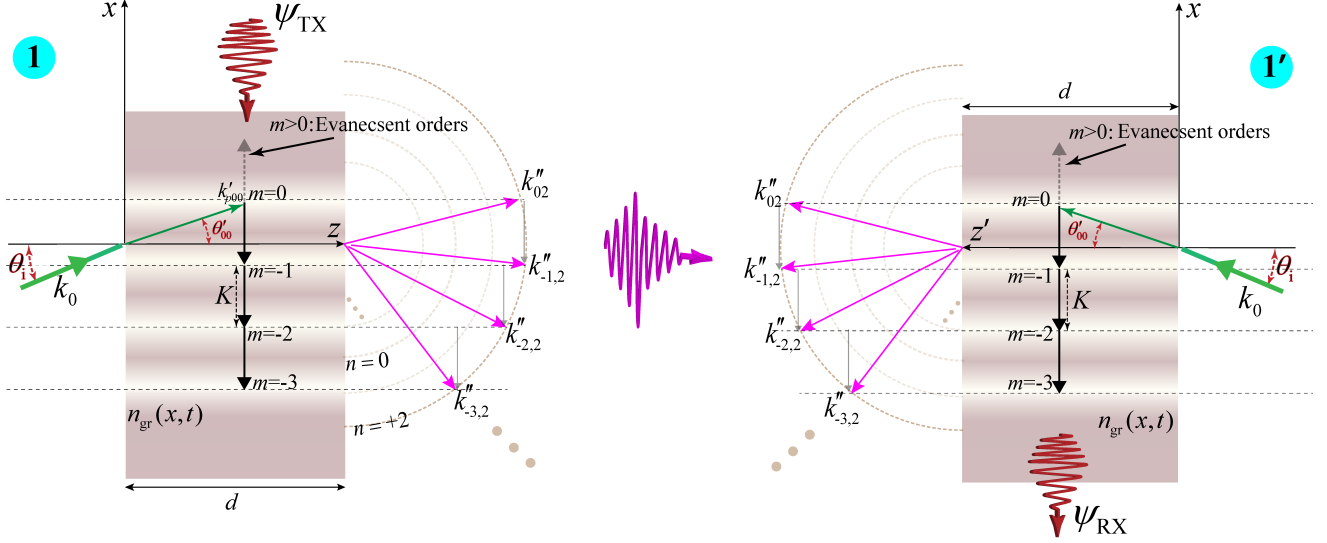


FIG. 12. Illustrative wavevector diagram of a particular transceiver pair in the space-time diffraction code multiple access system in Fig. 10.

- [2] M. Moharam and T. Gaylord, "Three-dimensional vector coupled-wave analysis of planar-grating diffraction," *J. Opt. Soc. Am.*, vol. 73, no. 9, pp. 1105–1112, 1983.
- [3] T. K. Gaylord and M. Moharam, "Analysis and applications of optical diffraction by gratings," *Proc. IEEE*, vol. 73, no. 5, pp. 894–937, 1985.
- [4] E. G. Loewen and E. Popov, *Diffraction gratings and applications*. CRC Press, 1997.
- [5] Y. Xu, Y. Fu, and H. Chen, "Steering light by a sub-wavelength metallic grating from transformation optics," *Sci. Rep.*, vol. 5, p. 12219, 2015.
- [6] N. Bonod and J. Neaupont, "Diffraction gratings: from principles to applications in high-intensity lasers," *Advances in Optics and Photonics*, vol. 8, no. 1, pp. 156–199, 2016.
- [7] M. Memarian and G. V. Eleftheriades, "Evanescent-to-propagating wave conversion in sub-wavelength metal-strip gratings," *IEEE Trans. Microw. Theory Techn.*, vol. 60, no. 12, pp. 3893–3907, 2012.
- [8] M. Memarian and G. V. Eleftheriades, "Enhanced radiation of an invisible array of sources through a sub-wavelength metal-strip grating and applications," *J. Appl. Phys.*, vol. 114, no. 13, p. 134902, 2013.
- [9] T. Tamir, H. Wang, and A. A. Oliner, "Wave propagation in sinusoidally stratified dielectric media," *IEEE Trans. Microw. Theory Techn.*, vol. 12, no. 3, pp. 323–335, 1964.
- [10] C. Burckhardt, "Diffraction of a plane wave at a sinusoidally stratified dielectric grating," *J. Opt. Soc. Am.*, vol. 56, no. 11, pp. 1502–1508, 1966.
- [11] M. G. Moharam, E. B. Grann, D. A. Pommet, and T. K. Gaylord, "Formulation for stable and efficient implementation of the rigorous coupled-wave analysis of binary gratings," *J. Opt. Soc. Am. A*, vol. 12, no. 5, pp. 1068–1076, 1995.
- [12] M. C. Hutley, "Diffraction gratings," *Techniques of Physics, London: Academic Press, 1982*, 1982.
- [13] C. Newswanger, "Holographic diffraction grating patterns and methods for creating the same," Mar. 1 1994. US Patent 5,291,317.
- [14] H. M. Smith, *Holographic recording materials*, vol. 20. Springer Science & Business Media, 2006.
- [15] W. B. Veldkamp, "Laser beam profile shaping with interlaced binary diffraction gratings," *Appl. Opt.*, vol. 21, no. 17, pp. 3209–3212, 1982.
- [16] K. Preston, "Coherent optical computers," 1972.
- [17] P. Chavel, A. A. Sawchuk, T. C. Strand, A. R. Tanguay, and B. H. Soffer, "Optical logic with variable-grating-mode liquid-crystal devices," *Opt. Lett.*, vol. 5, no. 9, pp. 398–400, 1980.
- [18] H. Eichler, G. Salje, and H. Stahl, "Thermal diffusion measurements using spatially periodic temperature distributions induced by laser light," *J. Appl. Phys.*, vol. 44, no. 12, pp. 5383–5388, 1973.
- [19] D. W. Phillion, D. J. Kuizenga, and A. E. Siegman, "Sub-nanosecond relaxation time measurements using a transient induced grating method," *Appl. Phys. Lett.*, vol. 27, no. 2, pp. 85–87, 1975.
- [20] D. L. Hecht, "Spectrum analysis using acousto-optic devices," *Opt. Eng.*, vol. 16, no. 5, p. 165461, 1977.
- [21] T. Suhara, H. Nishihara, and J. Koyama, "A folded-type integrated-optic spectrum analyzer using butt-coupled chirped grating lenses," *IEEE J. Quantum Electron.*, vol. 18, no. 7, pp. 1057–1059, 1982.
- [22] E. S. Cassedy, "Waves guided by a boundary with time-space periodic modulation," in *Proceedings of the Institution of Electrical Engineers*, vol. 112, pp. 269–279, IET, 1965.
- [23] E. S. Cassedy, "Dispersion relations in time-space periodic media: part II-unstable interactions," *Proc. IEEE*, vol. 55, pp. 1154 – 1168, Jul. 1967.
- [24] Z. Yu and S. Fan, "Complete optical isolation created by indirect interband photonic transitions," *Nat. Photonics*, vol. 3, pp. 91 – 94, Jan. 2009.
- [25] H. Qu, Z.-L. Deck-Léger, C. Caloz, and M. Skorobogatiy, "Frequency generation in moving photonic crystals," *J. Opt. Soc. Am. B*, vol. 33, no. 8, pp. 1616–1626, 2016.
- [26] S. Taravati, N. Chamanara, and C. Caloz, "Nonreciprocal electromagnetic scattering from a periodically space-

- time modulated slab and application to a quasisonic isolator,” *Phys. Rev. B*, vol. 96, p. 165144, Oct. 2017.
- [27] S. Taravati, “Giant linear nonreciprocity, zero reflection, and zero band gap in equilibrated space-time-varying media,” *Phys. Rev. Appl.*, vol. 9, p. 064012, Jun. 2018.
- [28] M. M. Salary, S. Jafar-Zanjani, and H. Mosallaei, “Time-varying metamaterials based on graphene-wrapped microwires: Modeling and potential applications,” *Phys. Rev. B*, vol. 97, no. 11, p. 115421, 2018.
- [29] D. Correias-Serrano, A. Alù, and J. Gomez-Diaz, “Magnetic-free nonreciprocal photonic platform based on time-modulated graphene capacitors,” *Phys. Rev. B*, vol. 98, no. 16, p. 165428, 2018.
- [30] Z. Wu and A. Grbic, “A transparent, time-modulated metasurface,” in *2018 12th International Congress on Artificial Materials for Novel Wave Phenomena (Metamaterials)*, pp. 439–441, IEEE, 2018.
- [31] S. Taravati and A. A. Kishk, “Advanced wave engineering via obliquely illuminated space-time-modulated slab,” *IEEE Trans. Antennas Propagat.*, vol. 67, no. 1, pp. 270–281, 2019.
- [32] S. Inampudi, M. M. Salary, S. Jafar-Zanjani, and H. Mosallaei, “Rigorous space-time coupled-wave analysis for patterned surfaces with temporal permittivity modulation,” *Optical Materials Express*, vol. 9, no. 1, pp. 162–182, 2019.
- [33] S. Y. Elnaggar and G. N. Milford, “Generalized space-time periodic circuits for arbitrary structures,” *arXiv preprint arXiv:1901.08698*, 2019.
- [34] S. Taravati and A. A. Kishk, “Dynamic modulation yields one-way beam splitting,” *Phys. Rev. B*, vol. 99, p. 075101, Jan. 2019.
- [35] J. R. Zurita-Sánchez, P. Halevi, and J. C. Cervantes-Gonzalez, “Reflection and transmission of a wave incident on a slab with a time-periodic dielectric function,” *Phys. Rev. A*, vol. 79, no. 5, p. 053821, 2009.
- [36] J. S. Martínez-Romero and P. Halevi, “Parametric resonances in a temporal photonic crystal slab,” *Phys. Rev. A*, vol. 98, no. 5, p. 053852, 2018.
- [37] P. K. Tien, “Parametric amplification and frequency mixing in propagating circuits,” *J. Appl. Phys.*, vol. 29, pp. 1347–1357, Sept. 1958.
- [38] E. S. Cassedy and A. A. Oliner, “Dispersion relations in time-space periodic media: part I-stable interactions,” *Proc. IEEE*, vol. 51, no. 10, pp. 1342 – 1359, 1963.
- [39] A. L. Cullen, “A travelling-wave parametric amplifier,” *Nature*, vol. 181, p. 332, Feb. 1958.
- [40] P. Tien and H. Suhl, “A traveling-wave ferromagnetic amplifier,” *Proc. IEEE*, vol. 46, no. 4, pp. 700–706, 1958.
- [41] J. Wentz, “A nonreciprocal electrooptic device,” *Proc. IEEE*, vol. 54, no. 1, pp. 97–98, 1966.
- [42] S. Bhandare, S. K. Ibrahim, D. Sandel, H. Zhang, F. Wust, and R. Noé, “Novel nonmagnetic 30-db traveling-wave single-sideband optical isolator integrated in III/V material,” *IEEE J. Sel. Top. Quantum Electron.*, vol. 11, no. 2, pp. 417–421, 2005.
- [43] H. Lira, Z. Yu, S. Fan, and M. Lipson, “Electrically driven nonreciprocity induced by interband photonic transition on a silicon chip,” *Phys. Rev. Lett.*, vol. 109, p. 033901, Jul. 2012.
- [44] N. A. Estep, D. L. Sounas, J. Soric, and A. Alù, “Magnetic-free non-reciprocity and isolation based on parametrically modulated coupled-resonator loops,” *Nat. Phys.*, vol. 10, no. 12, pp. 923–927, 2014.
- [45] N. Chamanara, S. Taravati, Z.-L. Deck-Léger, and C. Caloz, “Optical isolation based on space-time engineered asymmetric photonic bandgaps,” *Phys. Rev. B*, vol. 96, p. 155409, Oct. 2017.
- [46] S. Taravati, “Self-biased broadband magnet-free linear isolator based on one-way space-time coherency,” *Phys. Rev. B*, vol. 96, p. 235150, Dec. 2017.
- [47] Y. Hadad, D. L. Sounas, and A. Alù, “Space-time gradient metasurfaces,” *Phys. Rev. B*, vol. 92, no. 10, p. 100304, 2015.
- [48] Z. Yu and S. Fan, “Dynamic non-reciprocal meta-surfaces with arbitrary phase reconfigurability based on photonic transition in meta-atoms,” *Appl. Phys. Lett.*, vol. 108, p. 021110, 2009.
- [49] Y. Shi, S. Han, and S. Fan, “Optical circulation and isolation based on indirect photonic transitions of guided resonance modes,” *ACS Photonics*, vol. 4, pp. 1639–1645, Jun. 2017.
- [50] S. Taravati, “Aperiodic space-time modulation for pure frequency mixing,” *Phys. Rev. B*, vol. 97, no. 11, p. 115131, 2018.
- [51] H. Shanks, “A new technique for electronic scanning,” *IEEE Trans. Antennas Propag.*, vol. 9, no. 2, pp. 162–166, 1961.
- [52] S. Taravati and C. Caloz, “Space-time modulated nonreciprocal mixing, amplifying and scanning leaky-wave antenna system,” in *IEEE AP-S Int. Antennas Propagat. (APS)*, (Vancouver, Canada), 2015.
- [53] Y. Hadad, J. C. Soric, and A. Alù, “Breaking temporal symmetries for emission and absorption,” *Proc. Natl. Acad. Sci.*, vol. 113, no. 13, pp. 3471–3475, 2016.
- [54] D. Ramaccia, D. L. Sounas, A. Alù, F. Bilotti, and A. Toscano, “Nonreciprocity in antenna radiation induced by space-time varying metamaterial cloaks,” *IEEE Antennas Wirel. Propagat. Lett.*, vol. 17, no. 11, pp. 1968–1972, 2018.
- [55] M. M. Salary, S. Jafar-Zanjani, and H. Mosallaei, “Non-reciprocal optical links based on time-modulated nanoantenna arrays: Full-duplex communication,” *Phys. Rev. B*, vol. 99, no. 4, p. 045416, 2019.
- [56] A. Shlivinski and Y. Hadad, “Beyond the bode-fano bound: Wideband impedance matching for short pulses using temporal switching of transmission-line parameters,” *Phys. Rev. Lett.*, vol. 121, no. 20, p. 204301, 2018.
- [57] S. Taravati and C. Caloz, “Mixer-duplexer-antenna leaky-wave system based on periodic space-time modulation,” *IEEE Trans. Antennas Propagat.*, vol. 65, pp. 442 – 452, Feb. 2017.
- [58] L. Felsen and G. Whitman, “Wave propagation in time-varying media,” *IEEE Trans. Antennas Propag.*, vol. 18, no. 2, pp. 242–253, 1970.
- [59] F. Biancalana, A. Amann, A. V. Uskov, and E. P. Oreilly, “Dynamics of light propagation in spatiotemporal dielectric structures,” *Phys. Rev. E*, vol. 75, no. 4, p. 046607, 2007.
- [60] V. Bacot, M. Labousse, A. Eddi, M. Fink, and E. Fort, “Time reversal and holography with spacetime transformations,” *Nat. Phys.*, vol. 12, no. 10, p. 972, 2016.
- [61] F. R. Morgenthaler, “Velocity modulation of electromagnetic waves,” *IEEE Trans. Microw. Theory Tech.*, vol. 6, no. 2, pp. 167–172, 1958.
- [62] R. Fante, “Transmission of electromagnetic waves into time-varying media,” *IEEE Trans. Antennas Propagat.*, vol. 19, no. 3, pp. 417–424, 1971.

- [63] Z.-L. Deck-Léger, *Scattering in Space-Time Abruptly Modulated Structures*. PhD thesis, École Polytechnique de Montréal, 2017.
- [64] R. Costen and D. Adamson, “Three-dimensional derivation of the electrodynamic jump conditions and momentum-energy laws at a moving boundary,” *Proc. IEEE*, vol. 53, no. 9, pp. 1181–1196, 1965.
- [65] Bolotovskii, “Reflection of light from a moving mirror and related problems,”
- [66] E. Cassedy and A. Oliner, “Dispersion relations in time-space periodic media: part i: stable interactions,” *Proc. IEEE*, vol. 51, no. 10, pp. 1342–1359, 1963.
- [67] D. L. Sounas and A. Alù, “Non-reciprocal photonics based on time modulation,” *Nat. Photonics*, vol. 11, no. 12, p. 774, 2017.
- [68] C. Caloz, A. Alù, S. Tretyakov, D. Sounas, K. Achouri, and Z.-L. Deck-Léger, “Electromagnetic nonreciprocity,” *Phys. Rev. Appl.*, vol. 10, no. 4, p. 047001, 2018.
- [69] A. Merkel, M. Willatzen, and J. Christensen, “Dynamic nonreciprocity in loss-compensated piezophononic media,” *Phys. Rev. Appl.*, vol. 9, no. 3, p. 034033, 2018.
- [70] N. Glass, “Nonreciprocal diffraction via grating coupling to surface magnetoplasmons,” *Phys. Rev. B*, vol. 41, no. 11, p. 7615, 1990.
- [71] R. Birabassov, A. Yesayan, and T. V. Galstyan, “Nonreciprocal diffraction by spatial modulation of absorption and refraction,” *Opt. Lett.*, vol. 24, no. 23, pp. 1669–1671, 1999.
- [72] A. Potts, W. Zhang, and D. Bagnall, “Nonreciprocal diffraction through dielectric gratings with two-dimensional chirality,” *Phys. Rev. A*, vol. 77, no. 4, p. 043816, 2008.
- [73] O. Udalov, M. Sapozhnikov, E. Karashtin, B. Gribkov, S. Gusev, E. Skorohodov, V. Rogov, A. Y. Klimov, and A. Fraerman, “Nonreciprocal light diffraction by a lattice of magnetic vortices,” *Phys. Rev. B*, vol. 86, no. 9, p. 094416, 2012.
- [74] T.-J. Guo, T.-F. Li, M. Yang, H.-X. Cui, Q.-H. Guo, X.-W. Cao, and J. Chen, “Nonreciprocal optical diffraction by a single layer of gyromagnetic cylinders,” *Opt. Express*, vol. 22, no. 1, pp. 537–546, 2014.